ACS OMEGA

Open Access

http://pubs.acs.org/journal/acsodf

Article

In Situ Fabrication and Characterization of g-C_3N_4 onto Cellulose Nanofibers and Selective Separation of Heavy Metal Ions

Uzma Haseen, Sakshi Kapoor, Rais Ahmad Khan, Hilal Ahmad,* and Bon Heun Koo

Cite This: *ACS Omega* 2024, 9, 1620−1626

Read Online

ACCESS | Metrics & More | Article Recommendations

ABSTRACT: Graphitic carbon nitride nanosheets were synthesized onto cellulose nanofiber surfaces utilizing an eco-friendly salt melt approach. The fabricated material CNF@C_3N_4 selectively removes Ni(II) and Cu(II) from electroplating wastewater samples. The immobilization of g-C_3N_4 on solid substrates eases handling of nanomaterial in a flow-through approach and mitigates sorbent loss during column operations. Characterization techniques such as scanning electron microscopy, tunneling electron microscopy, and X-ray photoelectron microscopy were employed to analyze the surface morphology and chemical bonding within the synthesized material. Selective Cu(II) and Ni(II) sorption predominantly arises from the soft−soft interaction between metal ions and associated nitrogen groups. An inner-sphere surface complexation mechanism effectively elucidated the interaction dynamics between the metal and CNF@C_3N_4. Experimental findings demonstrated satisfactory separation of Ni(II) and Cu(II) ions, with the extraction of 340.0 and 385.0 mg g^{-1} of material, respectively. Additionally, the devised technique was executed for the preconcentration and quantification of trace metals ions in water samples with a detection limit and limit of quantification of 0.06 and 0.20 μg L^{-1}, respectively.

INTRODUCTION

The water pollution caused by organic and inorganic matters are categorized as a class 1 pollution.[1−3] Heavy metal pollution has become a major global environmental concern due to the element's toxicity and requires serious attention.[4−6] Despite being present in trace amounts, they have detrimental effects on human health.[7,8] The US Environmental Protection Agency has set a limit of 2.0−10 ppb for the amount of various heavy metals that are present in drinking water.[9] The World Health Organization (WHO) also recognizes their toxicity and promotes their removal, and monitoring their level in environmental water samples is one of its key priorities. Therefore, their extraction and separation from contaminated water streams is necessary before their discharge to natural water bodies.[10,11] On the other hand, at certain contaminated sites, the concentration level of heavy metals is low, and due to elemental interferences and sampling restrictions, detecting these elements at trace levels presents a formidable challenge when employing conventional methods such as atomic fluorescence spectrometry, X-ray fluorescence, cold vapor atomic absorption, graphite furnace atomic absorption spectroscopy, inductively coupled plasma optical emission spectroscopy, and inductively coupled plasma mass spectrometry.[12] To remove the concomitants and enhance the analyte sensitivity, a sample pretreatment procedure is frequently required. Solid-phase extraction (SPE) stands out as the favored, straightforward, and cost-effective approach for sample pretreatment. It offers the capability to attain substantial enrichment factors and ensures complete analyte retrieval. The separation and preconcentration of heavy metal ions have been successfully documented using a range of SPE sorbents including nanosorbents. Among these options, composite materials of silica, zeolites, metal−organic framework, graphene oxide, metal oxides, carbon nanotubes, and others have demonstrated exceptional suitability for SPE.[13−19] Nonetheless, advancements in coping with increasingly complex samples and the need for quicker analytical procedures necessitate ongoing efforts in the development of novel sorbents.

Graphitic carbon nitride (g-C_3N_4) has been widely studied for its application in a variety of fields, including photoconduction, hydrogen evolution, CO_2 capture, bioimaging, fuel cells, metal ion detection, and photocatalytic activity.[20−22] Up until now, numerous strategies have been used to prepare g-C3N4. The technique of pyrolysis, which uses organic chemicals containing carbon and nitrogen as precursors, is a simple approach and is frequently used.[23,24] In this experiment, g-C_3N_4 was produced onto a cellulose nanofiber surface using the salt melt method as opposed to conventional pyrolysis.[25,26] The straightforward procedure changed the solid-state reaction into a solid−liquid reaction that effectively mixed the reactants. Additionally, the morphology of the sample is uniform, the reaction time was speeded up, and it was simple to remove and collect the molten eutectic mixture for later use.

Here, we present a first-of-its-kind report on the column application of g-C_3N_4 nanosheets deposited onto the fiber

Received: October 18, 2023
Revised: November 28, 2023
Accepted: December 18, 2023
Published: December 27, 2023

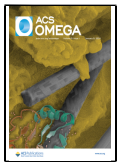

surface and employed in the removal of Ni(II) and Cu(II) from industrial wastewater (IWW) samples. We describe a straightforward method for composing g-C_3N_4 nanosheets on the surface of a nanocellulose fiber. The remarkable physicochemical attributes of 2-D g-C_3N_4 encompass porous structures, expansive specific surface areas, high crystalline quality, enhanced charge carrier separation, and numerous surface-active sites. When g-C_3N_4 nanosheets are deposited onto cellulose nanofibers, the g-C_3N_4 stacking is constrained, and a specific site for metal ion complexation is created. The structural defects observed may facilitate metal ions sorption by exposing extra nitrogen atoms that are present in the inner space and facilitate mass transfer.[1] The hybrid g-C_3N_4-deposited cellulose nanofibers demonstrate the effective removal of heavy metals in aqueous conditions. The X-ray photoelectron spectroscopy (XPS) analysis was used to discuss the mechanisms underlying the adsorption of heavy metal ions on g-C_3N_4. With a high adsorption capacity for heavy metals in our study, CNF@C_3N_4 stood out as having a significantly greater extraction efficiency than that of most other known nano adsorbents, including activated carbon, graphene oxide, and silica gel.

EXPERIMENTAL SECTION

Materials. Lithium chloride (LiCl), potassium chloride (KCl), and melamine ($C_3H_6N_6$) were procured and employed in the as-received form from Sigma-Aldrich. Copper nitrate and nickel nitrate salts were obtained from Sigma-Aldrich, and the metal ion solutions of desired concentration were prepared with deionized water (Milli-Q water (Merck)). Cellulose fibers were obtained from Biocrown Biotechnology (China) and utilized after rinsing with acetone, ethanol, and deionized water in this study.

Synthesis. Using the salt melt technique,[25,26] a molten eutectic mixture of LiCl and KCl (45/55 wt) was prepared by crushing LiCl and KCl to a fine powder. Then, in a glovebox, the molten eutectic mixture was completely mixed with melamine ($C_3H_6N_6$), and cellulose nanofibril (CNF) was employed as a precursor. The precursor solution was subsequently transferred into a 200 mL Teflon-lined hydrothermal vessel composed of stainless steel. This hydrothermal assembly was then placed in an air oven and heated at 200 °C for a duration of 12 h. The cellulose fibers were extracted after cooling, repeatedly rinsed with deionized water to eliminate unattached particles, and then dried at 60 °C in a vacuum oven for further characterization and application. Figure 1 illustrates the reaction scheme of the prepared sorbent.

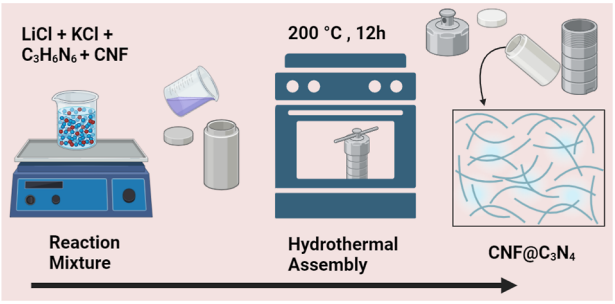

Figure 1. Schematic representation of preparation of the CNF@C_3N_4 sorbent.

General Column Procedure. Ni(II) and Cu(II) were separated from a model solution using a glass column that had particular measurements (length: 10 cm, diameter: 1 cm). The column was originally conditional using a buffer solution with a pH of 6.0 and filled with a prepared sorbent weighing 500 mg. Following that, 100 mL of the solution containing metal ions at the appropriate concentration and pH-adjusted to 6.0 was run through the column using a peristaltic pump at a flow rate of 6 mL per min. The filtrate was collected and subsequently analyzed by an inductively coupled plasma optical emission spectrometer precisely. The PerkinElmer Avio 200 model was used to measure the amount of metal ions in the filtrate.

Material Characterization. Modified cellulose nanofibrils' (CNF@C_3N_4) surface morphology was examined using a field emission scanning electron microscope model JSM-7800F manufactured by JEOL, (Kyoto, Japan). A TECNAI F30 S-Twin model high-resolution transmission electron microscope (Tokyo, Japan) was used to examine the high-resolution structure of CNF@C_3N_4. The sample was probe-sonicated into an ethanol suspension prior to high-resolution transmission electron microscopy (HRTEM) examination. Thermo Fisher Scientific's ESCALAB 250Xi equipment was used for XPS in order to analyze the surface elements. The XPS investigation utilized a MgK X-ray source with an energy of 1254.0 eV and a detection angle of 90°. The XPS experiments were conducted over the binding energy range 0−1400 eV, with a detection depth of approximately 10 nm.

RESULTS AND DISCUSSION

Characterization. Figure 2 presents the surface morphology of (CNFs) and the g-C_3N_4-modified CNF (CNF@C_3N_4) sorbent as observed through field emission scanning electron microscopy (FESEM). The successful incorporation of g-C_3N_4 nanoparticles onto the fiber surface is evident in the FESEM image of CNF@C_3N_4 in Figure 2B−D, displaying a distinct contrast compared to the surface of the initial fibers shown in Figure 2A. Figure 2E−G provides a high-resolution transmission electron microscopy (HRTEM) image of the g-C_3N_4 surface exhibiting a somewhat disordered atomic arrangement along the basal planes. Numerous dislocations and distortions are presented and impose an amorphous structure, as confirmed by the corresponding selected-area electron diffraction (SAED) pattern in Figure 2H. These defects possess the potential sites serving as additional diffusion pathways for Cu(II) and Ni(II) ions and thereby enhancing sorption capacity. The surface functional groups of CNF@C_3N_4 are characterized by Fourier transform infrared (FTIR) spectroscopy. As shown in Figure 3, the peak observed at 3400 cm^{-1} is attributed to the surface −OH groups of cellulose fibers in the CNF@C_3N_4 sorbent. Similarly, the peak observed at 2070 and 1630 cm^{-1} is attributed to stretching vibration of −C≡N and −C═N of the CNF@C_3N_4 sorbent, respectively. Additional substantiation of the g-C_3N_4 integration onto CNF is furnished by an XPS investigation. Figure 4A−C illustrates the deconvoluted core-level XPS spectra of C, N, and O functionalities. The nitrogen and oxygen surface functionalities are mainly responsible for the binding of metal ions during the adsorption process. The C 1s spectra at 285.0 eV (Figure 4A) reveal prominent peaks attributed to carbon characteristic of the carbon composition in the CNF@C_3N_4 sorbent. Likewise, Figure 4B showcases the deconvoluted nitrogen peaks at a binding energy of 399 eV, representing the N 2p1/2 and N 2p3/2 peaks originating from graphitic and pyrolytic nitrogen

https://doi.org/10.1021/acsomega.3c08177
ACS Omega 2024, 9, 1620−1626

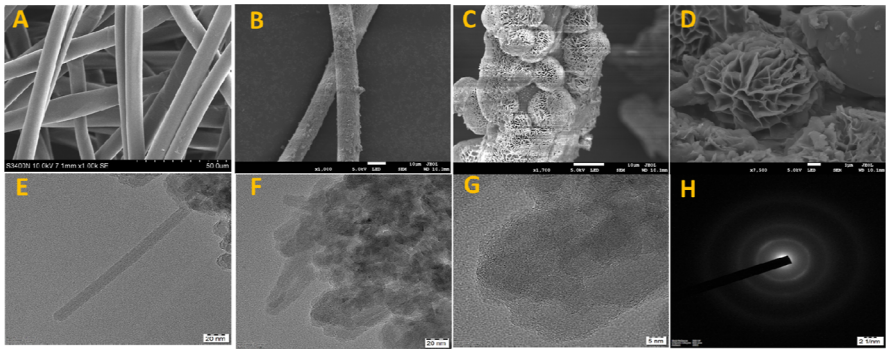

Figure 2. (A) Surface morphology of nascent CNFs observed under SEM; (B–D) surface morphology of the CNF@C_3N_4 sorbent at varying magnification with evident deposition of C_3N_4 sorbent onto CNF; (E–G) TEM images of CNF@C_3N_4 at varying positions and magnification; (H) SAED pattern of CNF@C_3N_4.

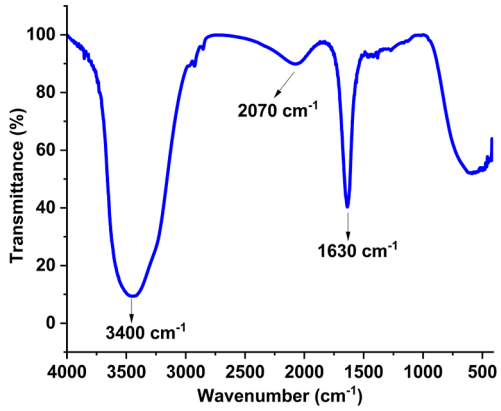

Figure 3. FTIR spectra of the CNF@C_3N_4 sorbent.

atoms within g-C_3N_4 integrated into the CNF@C_3N_4 sorbent. Figure 4C displays the deconvoluted core-level XPS peaks of oxygen atoms in g-C_3N_4 with binding energies of 532.4 and 530.5 eV, further affirming the immobilization of g-C_3N_4 onto the cellulose fiber surface.

Effect of Solution pH. The surface chemistry of the adsorbent is majorly dependent upon the solution pH. At acidic pH, the functional groups are positively charged due to protonation reaction and reject the cations upon contact. However, an opposite case was observed at a low acidic to basic pH value. We studied such effect on the adsorption of metal ions onto CNF@C_3N_4 at sample pH values from 2 to 7. We observed precipitates of Ni(II) and Cu(II), at solution pH of 8 and above, and therefore avoided. Significantly, in practical IWW, the pH typically falls within the acidic range, generally ranging from pH 4 to 6. Additionally, owing to its nitrogen-containing structure, the CNF@C_3N_4 material exhibits effective removal of Ni(II) and Cu(II) ions over a broader pH spectrum, spanning from 3 to 7, as depicted in Figure 5A. This broad pH range renders it suitable for treating water samples with varying pH levels, spanning from acidic to neutral. It is worth noting that at highly acidic conditions (pH 2), there is a decreased adsorption of metal ions. However, as the sample pH surpasses 3, the removal of metal ions demonstrates an increasing trend, culminating in maximum values of 340.0 and 385.0 mg g^{-1} for Ni(II) and Cu(II), respectively, within the pH range of 4–7 (Figure 5A). This rise in Ni(II) and Cu(II) adsorption at pH 6–7 is likely attributed to the formation of robust complexes with metal ions, facilitated by the nitrogen groups of the material. According to Pearson's hard and soft acid–base theory,[27,28] the lone pair of nitrogen vigorously coordinates with Ni(II) and Cu(II) ions, forming highly stable complexes. Furthermore, at lower sample pH levels, nitrogen becomes protonated, which makes it less likely to participate in metal complexation. Furthermore, zeta potential measurements of the CNF@C_3N_4 material were conducted at various pH values in the presence of monovalent ions as demonstrated in Figure 5B. It is evident that the point of zero charge occurs at pH of 3.6. When the pH falls below 3.6, the adsorbent material's surface starts to acquire a positive charge. Conversely, when the pH surpasses this value, the material's surface becomes negatively charged. Consequently, the exceptional capacity of the prepared material to remove

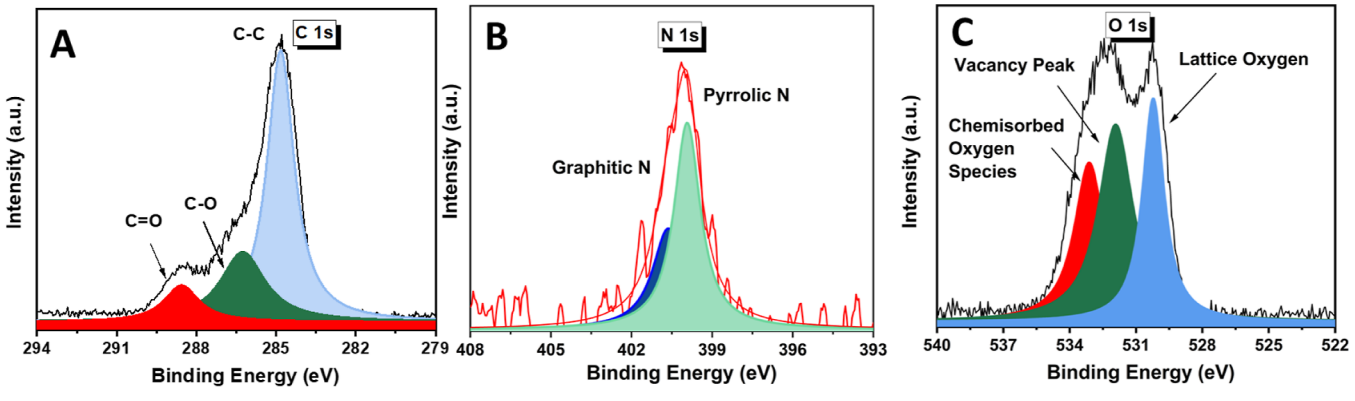

Figure 4. Illustration of the deconvoluted core-level XPS spectra of (A) carbon; (B) nitrogen; and (C) oxygen atoms of CNF@C_3N_4.

https://doi.org/10.1021/acsomega.3c08177
ACS Omega 2024, 9, 1620–1626

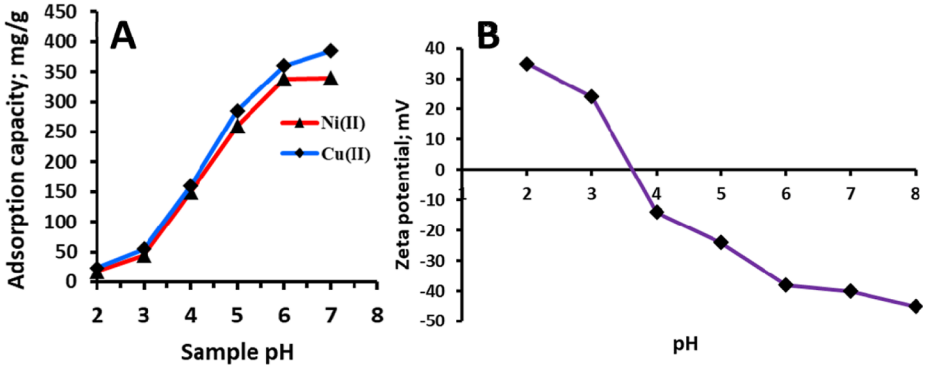

Figure 5. (A) Effect of solution pH on metal ion uptake; (B) zeta potential value of CNF@C_3N_4.

Ni(II) and Cu(II) ions within the pH range of 4.0−7.0 can be attributed to the strong electrostatic interactions and complexation between the positively charged divalent Ni(II) and Cu(II) ions and the negatively charged surface of the adsorbent material. Conversely, the reduction in the tendency of metal ions to adsorb at pH values lower than 3.5 is a consequence of electrostatic repulsion between the positively charged surface of the adsorbent material and the positively charged metal cations. Moreover, the effects of typical alkali and alkaline earth metals, which may coexist with Ni(II) and Cu(II) were also studied. Table 1 shows the tolerance level of

Table 1. Tolerance Level of Co-Existing Ions on the Separation of Studied Ions in Binary Mixture (Experimental Conditions: pH 6; Total Volume, 100 mL; Flow Rate, 6 mL min^{-1}; Metal Ions, 1000 $\mu g\ L^{-1}$)

added ions	tolerance ratio [added ions/metal ion] ($\mu g\ L^{-1}$)	recovery (%) Ni(II)	recovery (%) Cu(II)
Na^+ (NaCl)	6.82×10^4	97.5	98.9
K^+ (KCl)	4.45×10^4	97.8	98.0
NH_4^+ (NH_4Cl)	3.5×10^4	96.2	96.5
Ca^{2+}($CaCl_2$)	5.75×10^4	98.4	99.4
Mg^{2+}($MgCl_2$)	5.82×10^4	98.5	98.5
CH_3COO^- (CH_3COONa)	5.85×10^4	99.6	98.6
Cl^- (NaCl)	4.82×10^6	99.8	99.9
Br^- (NaBr)	4.65×10^6	99.5	99.5
SO_4^{2-} (Na_2SO_4)	5.50×10^5	97.9	98.9
CO_3^{2-} (Na_2CO_3)	5.00×10^5	99.2	99.5
NO_3^{2-} (Na_2NO_3)	5.80×10^5	99.4	99.8
humic acid	250	97.6	97.9
fulvic acid	250	99.0	99.5

coexisting ions toward the removal of Ni(II) and Cu(II) ions. It is clear that when compared to modified CNF@C_3N_4, nascent CNF showed relatively poor efficacy in the removal of Cu(II) and Ni(II) across all pH ranges. In contrast, CNF@C_3N_4 showed a good removal capacity for the studied ions. From solution pH 2−7, the removal of metal ions increased with increasing solution pH and reached to maximum removal capacity at a solution pH of 5−7. The nitrogen groups in CNF@C_3N_4 are highly favorable for the adsorption of Cu(II) and Ni(II) ions. These binding sites get protonated in very acidic environments, which results in reduced sorption of metal ions and decreases the removal capacity. At sample pH, the removal efficiency of CNF@C_3N_4 for Cu(II) and Ni(II) increases because of the high interaction between the nitrogen atoms and divalent metal ions as the sample pH rises. Due to the intrinsic nitrogen-rich characteristics, tiny particle size, and porous layered structure of CNF@C_3N_4, the prepared material exhibits a significant sorption tendency toward Cu(II) and Ni(II).

Preconcentration Studies and Breakthrough Volume. The direct quantification of heavy metal ions in environmental samples is a formidable task due to the extremely low levels of the target analyte and the interference caused by higher concentrations of coexisting anions and cations.[29] To overcome these challenges, preconcentration becomes essential as it serves to concentrate the analyte while simultaneously removing interfering ions from the treated sample. This work looked into the effectiveness of a CNF@C_3N_4 packed column for preconcentrating and analysis of studied ions. To study the dilution effect, a series of model solutions containing 1.0 μg of Cu(II) and Ni(II) with various volumes (from 1200 to 3200 mL) were prepared. Using a peristaltic pump, the sample solutions were percolated through a glass column at a flow rate of 6 mL min^{-1}. The adsorbed metal ions were then eluted and analyzed by inductively coupled plasma optical emission spectrometry (ICP-OES). A 3 mL portion of 0.5 M HCl acid was used as an eluent to completely elute the sorbed metal ions. Table 2 displays the findings of this preconcentration investigation. Significantly, Cu(II) and Ni(II) were preconcentrated with high quantitative recovery rates of 99.5 and 99.2%, respectively, when the sample volume was limited to 3000 mL. Nevertheless, when the sample volume was extended to 3200 mL, the recovery rates for Cu(II) and Ni(II) declined to 91.0 and 90.5%, respectively. The whole preconcentration procedure was repeated three times for individual metal ions, and the mean value of recovered analyte is considered. The preconcentration factor was determined as 1000, and the computed preconcentration limit for these metal ions was 0.33 $\mu g\ L^{-1}$. This means that, in addition to removing a high content of Cu(II) and Ni(II) from IWW, the proposed material can also successfully extract the lower amount of Cu(II) and Ni(II) from real samples. Furthermore, we investigated the breakthrough studies following the optimized procedure, where a sample solution of defined concentration, i.e., 10 mg L^{-1} of Cu(II) and Ni(II), were percolated through the column, and an aliquot at different time intervals was collected and analyzed for metal ion content to evaluate the breakthrough behavior. The breakthrough volume was defined as the volume of effluent where the metal ion concentration reached roughly 3−5% of the loading concentration, and the

https://doi.org/10.1021/acsomega.3c08177
ACS Omega 2024, 9, 1620−1626

Table 2. Preconcentration and Breakthrough Studies' Data (Column Parameters: Sample pH, 6; Flow Rate, 6 mL min^{-1}; Eluent Volume, 3 mL; Adsorbent Amount, 500 mg)

preconcentration studies				breakthrough studies	
sample volume (mL)	Ni(II) and Cu(II) ($\mu g\ L^{-1}$)	preconcentration limit ($\mu g\ L^{-1}$)	preconcentration factor	breakthrough volume (mL)	breakthrough capacity ($mg\ g^{-1}$)
1000	1.00	1.00	200	3800	Ni(II)-328.0 Cu(II) 355.0
1500	0.67	0.67	300		
2000	0.50	0.50	400		
2500	0.40	0.40	500		
2800	0.36	0.36	560		
3000	0.33	0.33	600		
3200	0.31				

same is illustrated in Figure 6. Furthermore, the total saturation volume obtained here was used to calculate the

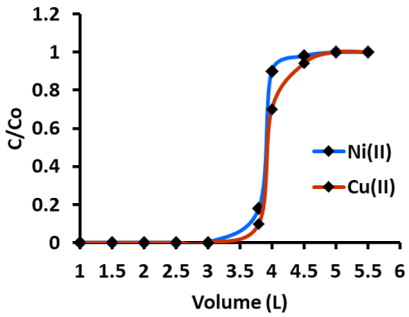

Figure 6. Breakthrough curve for Ni(II) and Cu(II) extraction.

maximum sorption capacity, which was then compared to the breakthrough capacity (Table 2). The suitability of the sorbent for use in the column technique is demonstrated by the close resemblance between the dynamic capacity, which closely approaches the breakthrough capacity, and the substantial preconcentration factor.

Optimization of Sample Flow Rate. The rate of sample flow through the column is an important factor to optimize since it affects the equilibrium established between the binding sites and metal ions at the solid−liquid interface. An optimum sample flow provides the complete sorption of metal ions onto a solid support. We studied and optimized the sample flow by percolating the sample solution through the packed column at varying flow rates. The retained analyte was then eluted and subsequently analyzed for complete retention of the loaded amount. An ideal flow rate enables for enough contact time between the sorbent's binding sites and the metal ions, which leads to effective extraction. Here, a sample solution of 1.0 mg L^{-1} concentration [Cu(II) and Ni(II)] set at pH 6.0 was passed through the column at different flow rates ranging from 4 to 10 mL min^{-1}. Afterward, the sorbed metal ions were eluted and determined by ICP-OES. Figure 7 illustrates the obtained data. It was found that the sorption of Cu(II) and Ni(II) ions gradually decreased to below 92% as the flow rate increased to 8.0 mL min^{-1}. The complete sorption of both metal ions was observed up to a sample flow of 6.0 mL min^{-1}. Hence, a sample flow rate of 6.0 mL min^{-1} was optimized and opted for real-sample analyses.

Analytical Method Validation. To determine whether the proposed analytical method is precise and produces accurate analytical results, we studied its precision and validated it by analyzing real samples of a known amount.

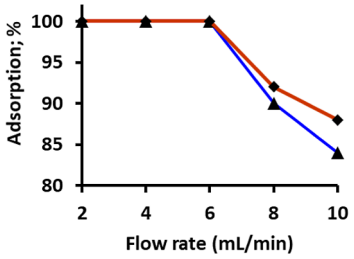

Figure 7. Effect of the sample flow rate on the extraction of Ni(II) and Cu(II).

Initially, we obtained a calibration plot by preconcentrating a range of solutions spanning from 0.0 to 100 ppb, which included a blank, following the meticulously optimized experimental procedure. This yielded a good level of linearity and a high correlation coefficient (R^2 = 0.9999). To determine the limit of detection (LOD) and limit of quantification (LOQ) in accordance with the IUPAC guidelines,[30] we use the formula CL = kS_b, where CL represents the concentration value for LOD and LOQ, K signifies the confidence level for LOD and LOQ, set at 99.96%, and S_b stands for the standard deviation of the mean blank signal. The method's sensitivity for real-sample analysis was demonstrated by the computed LOD values, which were determined to be 0.06 and 0.20 $\mu g\ L^{-1}$ for Cu(II) and Ni(II), respectively. The precision of the proposed method was found to be 3.5 and 3.8% for Cu(II) and Ni(II), respectively, analyzed for 10 consecutive measurements of a 1.0 $\mu g\ L^{-1}$ metal ion solution. This demonstrates the precision of the procedure by indicating the allowable closeness of the repeated measurements. Further, the proposed material was applied in the separation of metal ions from real samples. The alignment observed between the measured outcomes and the reported amounts of Cu(II) and Ni(II) ions, as presented in Table 3, speaks to the precision of the developed method, with a relative standard deviation (RSD) of less than 5%.

Optimization of Stripping Agent. To desorb the sorbed metal ions and prepare the column bed for the next sorption cycle, it is imperative to employ an appropriate eluting agent. In this study, we explored various mineral acids, including hydrochloric acid, nitric acid, and sulfuric acid, at concentrations of 0.25 and 2 M, using different volumes of 2, 3, and 5 mL to determine the optimal eluent type and concentration. The results indicate that Cu(II) and Ni(II) were efficiently recovered from all tested eluent solutions at higher concentrations and varying volumes. However, it is worth noting that when the eluent was lower (0.25 M), the recovery of Cu(II) and Ni(II) fell below 90%, except for the case of 3

https://doi.org/10.1021/acsomega.3c08177
ACS Omega 2024, 9, 1620−1626

Table 3. Application of CNF@C_3N_4 for the Separation of Ni(II) and Cu(II) Ions from IWW Samples (Sample Volume, 500 mL; Adsorbent Amount, 500 mg; Flow Rate, 6 mL min^{-1})

	amount measured (mg L^{-1}) ± standard deviation N = 3				
	Ni(II)		Cu(II)		
samples	before treatment	after treatment (removal %)	before treatment	after treatment (removal %)	RSD (%)
IWW 1	55.8 ± 3.20	0.005 ± 0.004 (99.95)	21.6 ± 1.53	0.003 ± 0.001 (99.97)	3.74
IWW 2	48.0 ± 2.25	0.002 ± 0.001 (99.95)	13.6 ± 1.23	0.002 ± 0.002 (99.99)	4.05
IWW 3	25.8 ± 3.20	0.008 ± 0.002 (99.99)	8.6 ± 0.58	0.000 ± 0.0001 (100)	3.47

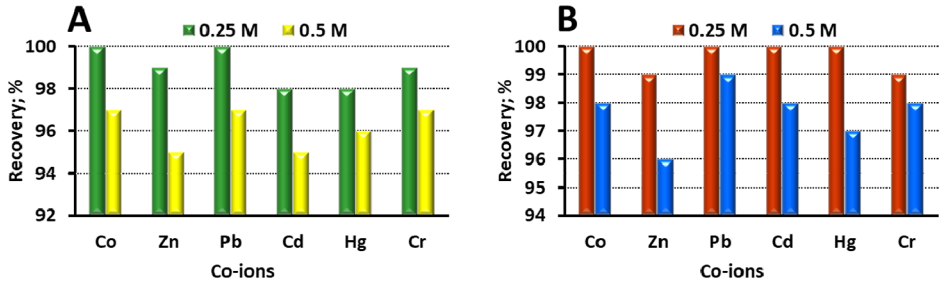

Figure 8. Effect of co-ions on the removal of (A) Ni(II) and (B) Cu(II) analyte ions.

mL of 0.5 M hydrochloric acid, which exhibited a recovery exceeding 99.9%. These findings led to the conclusion that a 3 mL volume of 0.5 M hydrochloric acid stands out as the most effective eluent for rejuvenating the column and preparing it for the subsequent sorption cycle.

Selectivity Studies. A series of binary mixture solutions containing common heavy metal ions, namely, Zn(II), Hg(II), Cd(II), Co(II), and Pb(II), were passed through a column to investigate their impact on the sorption of Cu(II) and Ni(II). The concentrations of Cu(II) and Ni(II) were maintained at 1.0 M within the 100 mL sample, while the concentrations of the other metal ions were set at 0.25 and 0.5 M. The assessment of the eluted sorbed Cu(II) and Ni(II) concentrations was conducted using ICP-OES. The results, depicted in Figure 8, reveal that there were no significant interferences observed in the extraction of Cu(II) and Ni(II) in the presence of these other metal ions, with analyte recoveries ranging from 95 to 99%. To establish a tolerance limit, defined as the highest co-ion concentration causing a variation in Cu(II) and Ni(II) recovery of less than 5%, it was found that the prepared sorbent exhibited strong selectivity for Cu(II) and Ni(II) over other divalent metal ions, as evidenced by its minimal sorption of competing ions. This remarkable selectivity could be attributed to the strong interaction between Cu(II) and Ni(II) and the −N atom present in CNF@C_3N_4, which is a component of the sorbent material. In conclusion, under carefully adjusted experimental conditions, successful recovery and quantification of Cu(II) and Ni(II) can be achieved even in the presence of other heavy metal ions at concentrations of up to 100 ppm, highlighting the method's capability for selective analysis in complex mixtures. Moreover, it is noteworthy that the efficiency of CNF@C_3N_4 for Cu(II) and/or Ni(II) extraction does not varying much. Under competitive conditions, the adsorption of Cu(II) ions are very close to Ni(II) adsorption.

CONCLUSIONS

The study effectively utilized g-C_3N_4 nanosheets immobilized on a CNF to concentrate and detect trace amounts of Cu(II) and Ni(II) in real samples. FESEM images provided clear evidence of the successful integration of g-C_3N_4 nanosheets onto the CNF surface, confirming the effectiveness of the immobilization process. Furthermore, the SAED pattern supported the HRTEM image, revealing a surface of g-C_3N_4 with numerous defects and a somewhat disordered atomic arrangement along the basal planes. These defects offered additional diffusion sites for Cu(II) and Ni(II) ions, thereby enhancing the sorbent's surface area and sorption capacity. The proposed technique displayed remarkable selectivity in capturing Cu(II) and Ni(II) and was relatively straightforward to implement. The key mechanism behind this successful binding and high affinity for Cu(II) and Ni(II) was attributed to the strong interaction between the nitrogen atom of g-C_3N_4 and the Cu(II) and Ni(II) ions. Crucially, the developed SPE method exhibited outstanding performance in quantitatively analyzing trace levels of Cu(II) and Ni(II) in drinking water and food samples, reaching parts per billion concentrations without being affected by common coexisting ions. Method validation was conducted by analyzing a standard reference material and employing the conventional addition procedure, thereby confirming the precision and reliability of the proposed method. In summary, the utilization of g-C_3N_4 in the SPE technique opens up new avenues for exploring other transition metal chalcogenides as potential sorbents for environmental monitoring and assessment applications.

AUTHOR INFORMATION

Corresponding Author

Hilal Ahmad − *Division of Computational Physics, Institute for Computational Science and Faculty of Applied Sciences, Ton Duc Thang University, Ho Chi Minh City 700000, Vietnam*; orcid.org/0000-0002-4870-3392; Email: hilalahmad@tdtu.edu.vn

Authors

Uzma Haseen − *Department of Chemistry, Aligarh Muslim University, Aligarh 202002, India*

Sakshi Kapoor − *Department of Physics, Indian Institute of Technology, New Delhi 110016, India*

Rais Ahmad Khan − *Department of Chemistry, College of Science, King Saud University, Riyadh 11451, Saudi Arabia*

https://doi.org/10.1021/acsomega.3c08177
ACS Omega 2024, 9, 1620−1626

Bon Heun Koo − *School of Materials Science and Engineering, Changwon National University, Changwon 1140 Gyeongnam, South Korea;* orcid.org/0000-0003-2867-056X

Complete contact information is available at: https://pubs.acs.org/10.1021/acsomega.3c08177

Notes

The authors declare no competing financial interest.

■ ACKNOWLEDGMENTS

The authors extend their thanks to Researchers Supporting Project (RSP2023R400), King Saud University (Riyadh, Saudi Arabia).

■ REFERENCES

(1) Haseen, U.; Ahmad, H. Preconcentration and Determination of Trace Hg(II) Using a Cellulose Nanofiber Mat Functionalized with MoS2 Nanosheets. *Ind. Eng. Chem. Res.* **2020**, *59* (7), 3198−3204.
(2) Liu, W.-J.; Li, W.-W.; Jiang, H.; Yu, H.-Q. Fates of Chemical Elements in Biomass during Its Pyrolysis. *Chem. Rev.* **2017**, *117* (9), 6367−6398.
(3) Samriti; Ojha, A.; Ojha, A.; Prakash, J. Water Challenges in South Asian Countries: A Focused Review on Emerging Nanomaterials and Technological Processes in Wastewater Treatment. *ACS ES&T Water* **2023**, *3* (6), 1463−1483.
(4) Hg, E. https://www.epa.gov/ground-water-and-drinking-water/national-primary-drinking-water-regulations#Inorganic (accessed on November 02, 2023).
(5) Hg, W. https://www.who.int/ipcs/assessment/public_health/mercury/en/. https://www.who.int/ipcs/assessment/public_health/mercury/en/ (accessed on November 02, 2023).
(6) Zhang, K.; Luo, X.; Yang, L.; Chang, Z.; Luo, S. Progress toward Hydrogels in Removing Heavy Metals from Water: Problems and Solutions—A Review. *ACS ES&T Water* **2021**, *1* (5), 1098−1116.
(7) Hou, D.; O'Connor, D.; Igalavithana, A. D.; Alessi, D. S.; Luo, J.; Tsang, D. C. W.; Sparks, D. L.; Yamauchi, Y.; Rinklebe, J.; Ok, Y. S. Metal contamination and bioremediation of agricultural soils for food safety and sustainability. *Nat. Rev. Earth Environ.* **2020**, *1* (7), 366−381.
(8) Kawata, K.; Yokoo, H.; Shimazaki, R.; Okabe, S. Classification of Heavy-Metal Toxicity by Human DNA Microarray Analysis. *Environ. Sci. Technol.* **2007**, *41* (10), 3769−3774.
(9) Wu, J.; Cao, M.; Tong, D.; Finkelstein, Z.; Hoek, E. M. V. A critical review of point-of-use drinking water treatment in the United States. *npj Clean Water* **2021**, *4* (1), 40.
(10) Dahaghin, Z.; Mousavi, H. Z.; Boutorabi, L. Application of magnetic ion-imprinted polymer as a new environmentally-friendly nonocomposite for a selective adsorption of the trace level of Cu(II) from aqueous solution and different samples. *J. Mol. Liq.* **2017**, *243*, 380−386.
(11) Femina Carolin, C.; Kamalesh, T.; Kumar, P. S.; Rangasamy, G. A Critical Review on the Sustainable Approaches for the Removal of Toxic Heavy Metals from Water Systems. *Ind. Eng. Chem. Res.* **2023**, *62* (22), 8575−8601.
(12) Ahmad, H.; Cai, C.; Liu, C. Separation and preconcentration of Pb(II) and Cd(II) from aqueous samples using hyperbranched polyethyleneimine-functionalized graphene oxide-immobilized polystyrene spherical adsorbents. *Microchem. J.* **2019**, *145*, 833−842.
(13) Li, J.-R.; Wang, X.; Yuan, B.; Fu, M.-L.; Cui, H.-J. Robust removal of heavy metals from water by intercalation chalcogenide [CH 3 NH 3]$_{2x}$ Mn$_x$ Sn$_{3-x}$ S 6·0.5H 2 O. *Appl. Surf. Sci.* **2014**, *320*, 112−119.
(14) Li, J.-R.; Wang, X.; Yuan, B.; Fu, M.-L. Layered chalcogenide for Cu2+ removal by ion-exchange from wastewater. *J. Mol. Liq.* **2014**, *200*, 205−212.
(15) Gao, M.-R.; Xu, Y.-F.; Jiang, J.; Yu, S.-H. Nanostructured metal chalcogenides: synthesis, modification, and applications in energy conversion and storage devices. *Chem. Soc. Rev.* **2013**, *42* (7), 2986−3017.
(16) Cheng, W.; Rechberger, F.; Niederberger, M. Three-Dimensional Assembly of Yttrium Oxide Nanosheets into Luminescent Aerogel Monoliths with Outstanding Adsorption Properties. *ACS Nano* **2016**, *10* (2), 2467−2475.
(17) Wang, L.; Wu, X.-L.; Xu, W.-H.; Huang, X.-J.; Liu, J.-H.; Xu, A.-W. Stable Organic−Inorganic Hybrid of Polyaniline/α-Zirconium Phosphate for Efficient Removal of Organic Pollutants in Water Environment. *ACS Appl. Mater. Interfaces* **2012**, *4* (5), 2686−2692.
(18) Rojas, S.; Horcajada, P. Metal−Organic Frameworks for the Removal of Emerging Organic Contaminants in Water. *Chem. Rev.* **2020**, *120* (16), 8378−8415.
(19) Kaur, J.; Sengupta, P.; Mukhopadhyay, S. Critical Review of Bioadsorption on Modified Cellulose and Removal of Divalent Heavy Metals (Cd, Pb, and Cu). *Ind. Eng. Chem. Res.* **2022**, *61* (5), 1921−1954.
(20) Wang, J.; Wang, S. A critical review on graphitic carbon nitride (g-C3N4)-based materials: Preparation, modification and environmental application. *Coord. Chem. Rev.* **2022**, *453*, 214338.
(21) Chen, Z.; Zhang, S.; Liu, Y.; Alharbi, N. S.; Rabah, S. O.; Wang, S.; Wang, X. Synthesis and fabrication of g-C3N4-based materials and their application in elimination of pollutants. *Sci. Total Environ.* **2020**, *731*, 139054.
(22) Huang, H.; Jiang, L.; Yang, J.; Zhou, S.; Yuan, X.; Liang, J.; Wang, H.; Wang, H.; Bu, Y.; Li, H. Synthesis and modification of ultrathin g-C3N4 for photocatalytic energy and environmental applications. *Renewable Sustainable Energy Rev.* **2023**, *173*, 113110.
(23) Inagaki, M.; Tsumura, T.; Kinumoto, T.; Toyoda, M. Graphitic carbon nitrides (g-C3N4) with comparative discussion to carbon materials. *Carbon* **2019**, *141*, 580−607.
(24) Ong, W.-J.; Tan, L.-L.; Ng, Y. H.; Yong, S.-T.; Chai, S.-P. Graphitic Carbon Nitride (g-C3N4)-Based Photocatalysts for Artificial Photosynthesis and Environmental Remediation: Are We a Step Closer To Achieving Sustainability? *Chem. Rev.* **2016**, *116* (12), 7159−7329.
(25) Liu, H.; Chen, D.; Wang, Z.; Jing, H.; Zhang, R. Microwave-assisted molten-salt rapid synthesis of isotype triazine-/heptazine based g-C3N4 heterojunctions with highly enhanced photocatalytic hydrogen evolution performance. *Appl. Catal., B* **2017**, *203*, 300−313.
(26) Villalobos, L. F.; Vahdat, M. T.; Dakhchoune, M.; Nadizadeh, Z.; Mensi, M.; Oveisi, E.; Campi, D.; Marzari, N.; Agrawal, K. V. Large-scale synthesis of crystalline g-C_3N_4 nanosheets and high-temperature H_2 sieving from assembled films. *Sci. Adv.* **2020**, *6* (4), No. eaay9851.
(27) Pearson, R. G. Hard and soft acids and bases, HSAB, part 1: Fundamental principles. *J. Chem. Educ.* **1968**, *45* (9), 581.
(28) Pearson, R. G. Hard and soft acids and bases, HSAB, part II: Underlying theories. *J. Chem. Educ.* **1968**, *45* (10), 643.
(29) Zhang, M.; Hu, J.; Tang, Q.; Zhang, J.; Jiang, X.; Hou, X. Phosphonic Acid-Functionalized MIL-53(Al) As an Efficient Sorbent for Trace Rare Earth Elements Preconcentration, Storage and Their Determination by X-ray Fluorescence Spectrometry. *Anal. Chem.* **2023**, *95* (38), 14169−14174.
(30) Long, G. L.; Winefordner, J. D. Limit of Detection A Closer Look at the IUPAC Definition. *Anal. Chem.* **1983**, *55* (07), 712A−724A.